JOM, Vol. 70, No. 10, 2018
https://doi.org/10.1007/s11837-018-3031-9

SOLUTION PURIFICATION TECHNOLOGY

Manganese Extraction from Low-Grade Pyrolusite by Roasting with H_2SO_4

FEI TENG,[1,2,3,4] SHAOHUA LUO,[2,3,4,6] WENNING MU,[1,2,3] XUEFEI LEI,[1,2,3] HAIXIA XIN,[1,2,3] YUCHUN ZHAI,[1,3] and YONGNIAN DAI[5]

1.—School of Metallurgy, Northeastern University, Shenyang 110819, China. 2.—School of Resources and Materials, Northeastern University at Qinhuangdao, Qinhuangdao 066004, China. 3.—Qinhuangdao Laboratory of Resources Cleaner Conversion and Efficient Utilization, Qinhuangdao 066004, China. 4.—Key Laboratory of Dielectric and Electrolyte Functional Material Hebei Province, Qinhuangdao 066004, China. 5.—Faculty of Metallurgical and Energy Engineering, Kunming University of Science and Technology, Kunming 650093, China. 6.—e-mail: tianyanglsh@163.com

A new method was studied for extracting manganese from low-grade pyrolusite with H_2SO_4 roasting and subsequent water leaching. The mechanism of roasting and optimal conditions for roasting, including the amounts of H_2SO_4 and H_2O addition and the roasting temperature and time, were discussed. The results indicated that the pyrolusite roasting process in the temperature range of 400–600°C was controlled by internal diffusion. The apparent activation energies in the time ranges of 0–30 min and 60–240 min were 25.26 kJ/mol and 14.94 kJ/mol, respectively. The maximum extraction of Mn reached approximately 98%, and the minimum extraction of Fe was approximately 1% under the optimal conditions. The ferric ion concentration was below 0.05 g/L in the leaching solution; thus, Mn was effectively separated from Fe and Si.

INTRODUCTION

Manganese ore mainly exists in the form of $MnCO_3$ and MnO_2 in nature.[1] Given the large-scale consumption of manganese carbonate ore, manganese oxide ore has become an important raw material.[2] There is a growing demand for manganese resources, but the lack of rich manganese ore has intensified the discrepancy between the manganese ore supply and demand.[3] The main component is MnO_2 in pyrolusite,[4] some of which is richly collected but poorly abandoned in production practice.[5] This practice produces low-grade pyrolusite tailings, causes environmental pollution and wastes resources. Therefore, economic development and utilization of low-grade pyrolusite are of great significance for sustainable development in the manganese industry and clean utilization of manganese ore resources.[6]

At present, there are four categories of methods for extracting manganese from pyrolusite: (1) reduction roasting followed by acid leaching using reductants such as bagasse,[3] cornstalk,[7] sulfur, coals, CO, pyrite, iron(II) sulfate[8] and sulfur dioxide;[9] (2) reduction roasting followed by water leaching;[2] (3) reductive acid leaching methods using various reductive agents,[10] such as glucose,[11] cane molasses,[12] sawdust,[13] oxalic,[14] waste tea,[15] hydrogen peroxide,[16] iron metal,[9] corncob,[17] CaS,[18] and ferrous sulfate or ferrous chloride;[9] (4) the bacterial-catalyzed two-ore method.[19]

Low-grade pyrolusite usually contains multiple elements. A successful method should effectively separate manganese from other elements.[2] The extraction methods for manganese, as mentioned above, are carried out under reducing conditions. The addition of reductants will introduce impurity elements and consequently increase the difficulty of the manganese purification. Using organic reductants to treat pyrolusite has been shown to be a pollution-free and feasible technique; however, there has been little commercial implementation of this technique due to the expense of the reductants and the high reductant consumption rate.[20]

(Published online July 11, 2018)

This article introduces a method for extracting manganese from low-grade pyrolusite from Gansu with H_2SO_4 roasting followed by water leaching. This process, without any reductants, is simple and easily controlled, and it effectively separates manganese from other elements.

MATERIALS AND METHODS

Materials

The low-grade pyrolusite used in the work was from Gansu. It was sieved to < 74 μm after being crushed and ground. All of the chemicals procured from local suppliers were analytical grade, and deionized water was used throughout.

Characterization

The main chemical composition of the pyrolusite is listed in Table I. The main mineral components were identified by x-ray diffraction (XRD, Rigaku SmartLab). The XRD pattern in Fig. 1a reveals that the major mineral phases include quartz, pyrolusite and hematite. The morphology of the sample was analyzed by scanning electron microscopy (SEM, Zeiss Supra 55). The SEM image in Fig. 1b shows that that the sample particle shape is irregular. The pyrolusite-roasting process was investigated by thermogravimetry coupled with differential scanning calorimetry (TG-DSC) with a thermal analysis instrument (Setsys Evo).

Experimental Procedure

For the roasting experiments, the schematic diagram of the experimental equipment is presented in Fig. 2. The pyrolusite sample, sulfuric acid and water were mixed according to a certain proportion in a corundum crucible and then roasted in a shaft furnace at a specified temperature for a certain period of time. The SO_3 gas generated during the roasting process was absorbed by dilute sulfuric acid and returned to the roasting vessel. For kinetic experiments on the roasting process, samples were taken out at regular intervals at fixed temperatures. When the roasting process was completed, the roasting clinker was removed and cooled to room temperature.

The roasting clinker and water were then placed into a leaching vessel. Once the set temperature was reached, the vessel was placed in a water bath with mechanical stirring for 50 min at 90°C. The solution was then filtered to separate the filtrate from the residue. The filtrate volume was measured, and the residue was washed with deionized water and dried. The content of Mn and Fe in the filtrate was determined by ammonium ferrous sulfate titration and dichromate titration, respectively.

RESULTS AND DISCUSSION

Thermodynamic Analysis and Phase Transformation of the Pyrolusite Roasting

The TG-DSC curve of the pyrolusite roasting process is shown in Fig. 3a. The samples were heated from 50°C to 900°C at 5°C/min. The reaction temperature for the pyrolusite and sulfuric acid was in the range of 100–300°C. The reaction peak at 400–500°C was due to the decomposition of $Fe_2(SO4)_3$. The decomposition temperatures of $MnSO_4$ occurred in the range of 700–800°C.

Figure 3b shows the XRD patterns of the raw material and the roasted products prepared at different temperatures. As shown in Fig. 3b, the diffraction intensities of the pyrolusite and hematite in the raw ore decreased at 300°C, and manganese sulfate and iron sulfate were generated according to the following equations:[21]

$$Fe_2O_3 + 3H_2SO_4 = Fe_2(SO_4)_3 + 3H_2O \quad (1)$$

$$H_2SO_4 = H_2O + SO_3 \uparrow \quad (2)$$

$$2MnO_2 + 2H_2SO_4 = 2MnSO_4 + 2H_2O + O_2 \uparrow \quad (3)$$

The size of the iron sulfate peak gradually increased with increasing roasting temperature (< 400°C) and then decreased (> 500°C) because hematite formed because of the decomposition of iron sulfate at 480°C:

$$Fe_2(SO_4)_3 = 3SO_3 \uparrow + Fe_2O_3 \quad (4)$$

The diffraction intensity of the manganese sulfate peak in the roasted products gradually increased as the roasting temperature increased up to 600°C. The diffraction intensity of the manganese sulfate peak decreased from 700°C to 800°C, and manganese oxide (Mn_2O_3) was detected in the roasting clinker at 800°C. Mn_2O_3 was generated because of the decomposition of $MnSO_4$. The decomposition reaction equations of $MnSO_4$ can be written as:[22,23]

$$2MnSO_4 = Mn_2O_3 + 2SO_2 \uparrow + 1/2O_2 \uparrow \quad (5)$$

$$2SO_2 \uparrow + O_2 \uparrow + 2H_2O = 2H_2SO_4 \quad (6)$$

Table I. Main chemical components of pyrolusite

Composition	MnO_2	Fe_2O_3	SiO_2	K_2O	CaO	Al_2O_3
Content (wt.%)	40.64	7.84	48.65	0.99	0.88	0.41

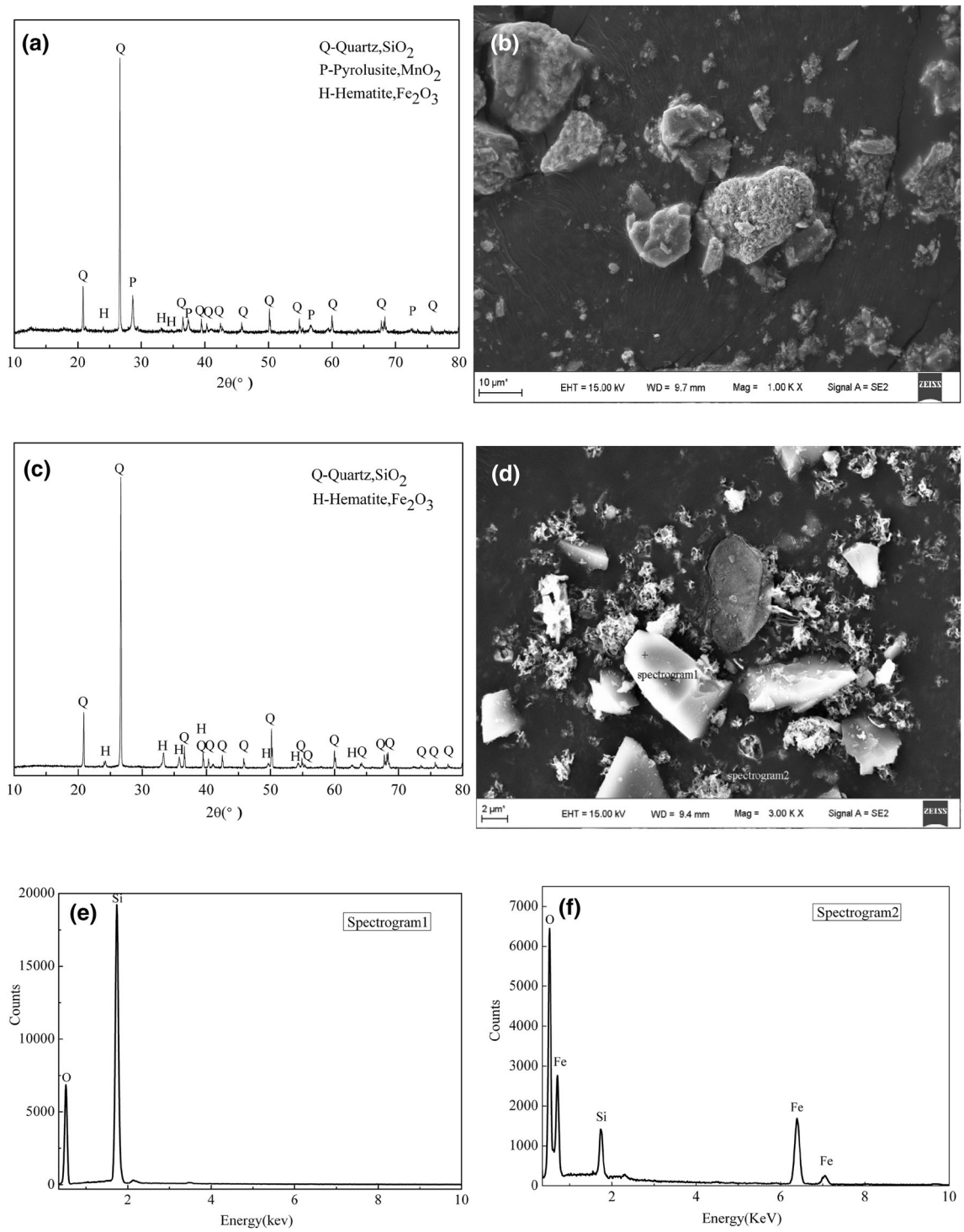

Fig. 1. (a, b) XRD pattern and SEM micrograph of the pyrolusite. (c, d) XRD pattern and SEM micrograph of the leaching residue. (e, f) EDS images of a micrograph of the leaching residue.

The position and intensity of the quartz peaks were nearly unchanged at all the roasting temperatures.

The relationship of $\Delta G^{\theta} - T$ is shown in Fig. 3g, $\Delta G^{\theta} - T$ based on the HSC chemistry 6.0. We can only use the ΔG^{θ} to roughly estimate reactions because of the uncertainty of the gas partial pressure in the system. Although the ΔG^{θ} of Eq. (4) is positive at 480°C, the presence of SO_3 makes the decomposition of $Fe_2(SO_4)_3$ easy. Similarly, the presence of SO_3 and O_2 in the system make the decomposition temperature of $MnSO_4$ decrease.

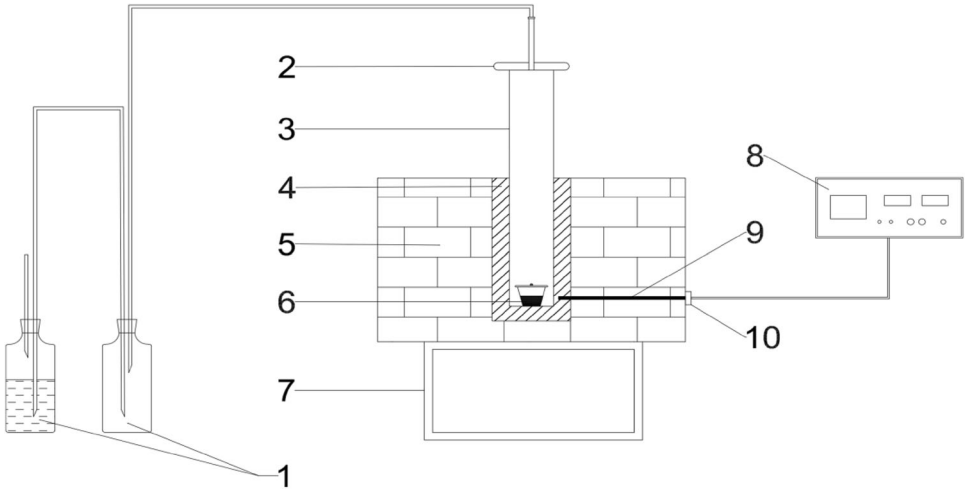

Fig. 2. Schematic diagram of the roasting equipment: *1* gas collector, *2* sealing ring, *3* tube of stainless steel, *4* heating element, *5* crucible resistance furnace, *6* crucible, *7* support frame, *8* electronic thermo-controllers, *9* thermocouple, and *10* terminal.

The Effect of the Roasting Conditions

The Effect of the H_2SO_4 to Pyrolusite Mass Ratio

The mass of H_2SO_4 consumed to completely react with the Fe_2O_3 and MnO_2 in pyrolusite was counted 1. The influence of the mass ratio of H_2SO_4 to pyrolusite was studied. The extraction of Mn and Fe increased with the addition of H_2SO_4, as shown in Fig. 3c. The Mn extraction increased slowly for mass ratios above 2:1 and resulted in a large volatilization of SO_3 as more H_2SO_4 was added. Therefore, the optimal mass ratio of H_2SO_4 to pyrolusite was 2:1.

The Effect of the Roasting Temperature

The effect of the roasting temperature is shown in Fig. 3d. The extraction of Mn increased rapidly as a function of the roasting temperature under 600°C, and the extraction of Fe increased similarly below 400°C. Increasing the temperature accelerates the reaction rate and improves the extraction. The extraction of Mn began to decrease when the roasting temperature exceeded 600°C, possibly because of the decomposition of $MnSO_4$. The extraction of Fe decreased sharply above 400°C because of the decomposition of $Fe_2(SO_4)_3$. Increasing the temperature will accelerate the sulfate decomposition and reduce the extraction efficiency. To separate manganese and iron, a high Mn recovery rate coupled with a low Fe extraction rate should be chosen; hence, the appropriate roasting temperature was 650°C.

The Effect of the H_2O to H_2SO_4 Volume Ratio

The effect of the H_2O to H_2SO_4 volume ratio on the extraction of Mn and Fe was also investigated, and the results are shown in Fig. 3e. The extraction of Fe increased as the volume ratio increased from 0:1 to 1:1, corresponding to the H_2SO_4 concentrations of 18.4 mol/L, 16.66 mol/L, 14.63 mol/L, 12.78 mol/L, 11.26 mol/L and 10.07 mol/L respectively. Increasing the H_2O to H_2SO_4 volume ratio up to 0.6:1 enhanced the Mn extraction. Increasing the system liquidity and contact area between the reactants promoted the reaction. The extraction of Mn began to decline when the ratio increased above 0.6:1 due to the low sulfuric acid concentration. When the ratio was below 0.6:1, there was little effect on the extraction of Mn. Given the demand for a higher Mn extraction and lower Fe extraction, the most favorable ratio was 0.2:1.

The Effect of the Roasting Time

Figure 3f presents the influence of the roasting time. The extraction of Fe decreased quickly from 0.5 h to 4 h and decreased slowly after 4 h because increasing the roasting time accelerated the decomposition of $Fe_2(SO_4)_3$. Furthermore, the extraction of Mn reached a maximum at 4 h. Increasing the reaction time is beneficial for the formation of manganese sulfate, but it accelerates the decomposition of $MnSO_4$ after 4 h. Thus, the optimum roasting time was 4 h.

Characterization of Leaching Residue

The XRD pattern of the leaching residue obtained under the optimal conditions is shown in Fig. 1c. The main phases in the leaching residue are SiO_2 and Fe_2O_3. The SEM micrographs and EDS images of the leaching residue are shown in Fig. 1d–f. The SiO_2 particles are lumpy, and the Fe_2O_3 particles are agglomerated. Compared with those of Fe_2O_3, the SiO_2 particles are larger.

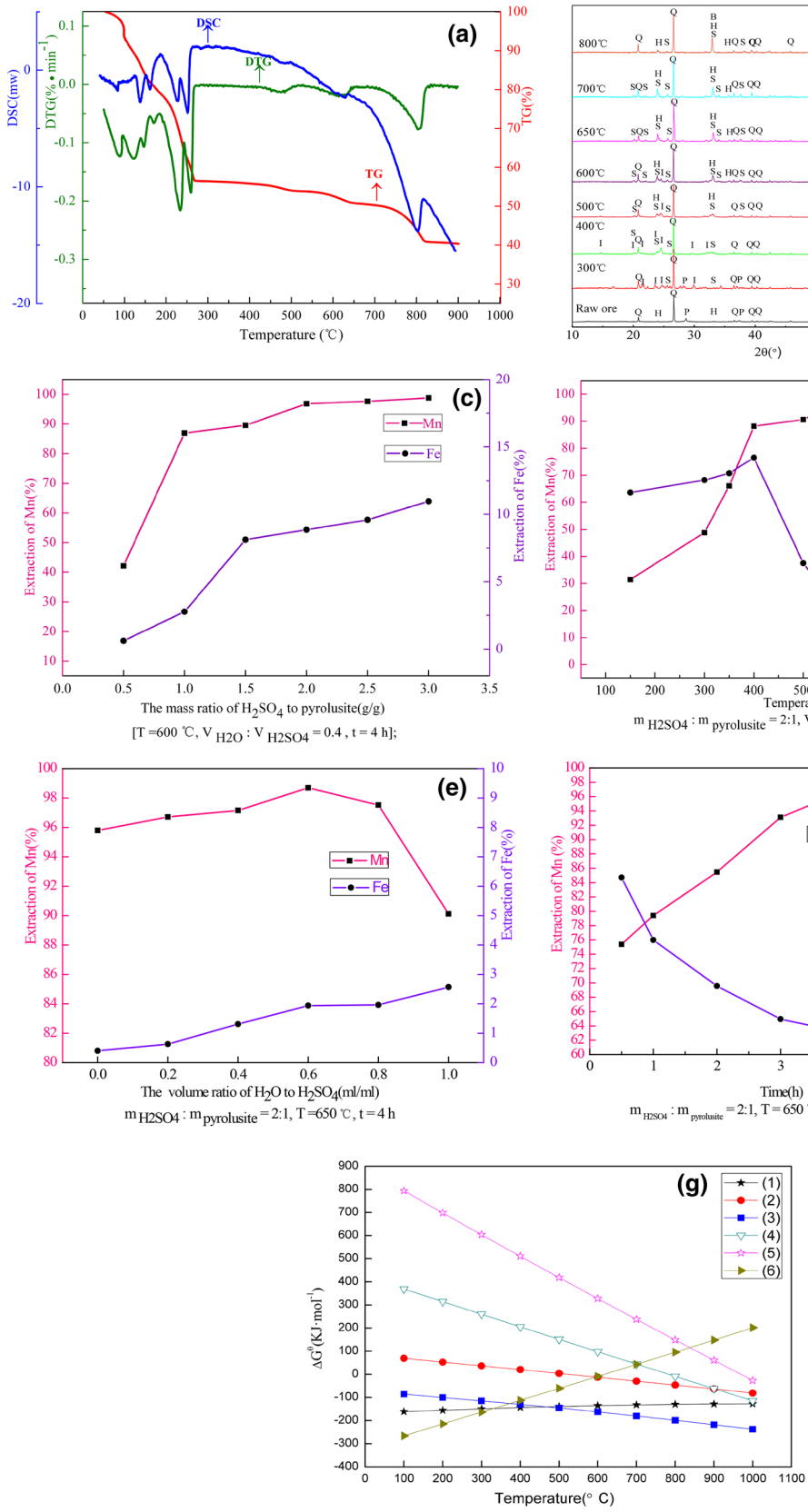

Fig. 3. (a) Thermal analysis of the pyrolusite roasting process. (b) XRD patterns of the products from pyrolusite roasting with sulfuric acid at different temperatures. (*H* hematite, Fe_2O_3, *P* pyrolusite, MnO_2, *Q* quartz, SiO_2, *S* manganese sulfate, $MnSO_4$, *I* iron sulfate, $Fe_2(SO_4)_3$, *B* manganese oxide, Mn_2O_3). (c–f) Effect of the roasting conditions. (g) The relationship of ΔG^{θ}-T corresponding reactions (1)–(6).

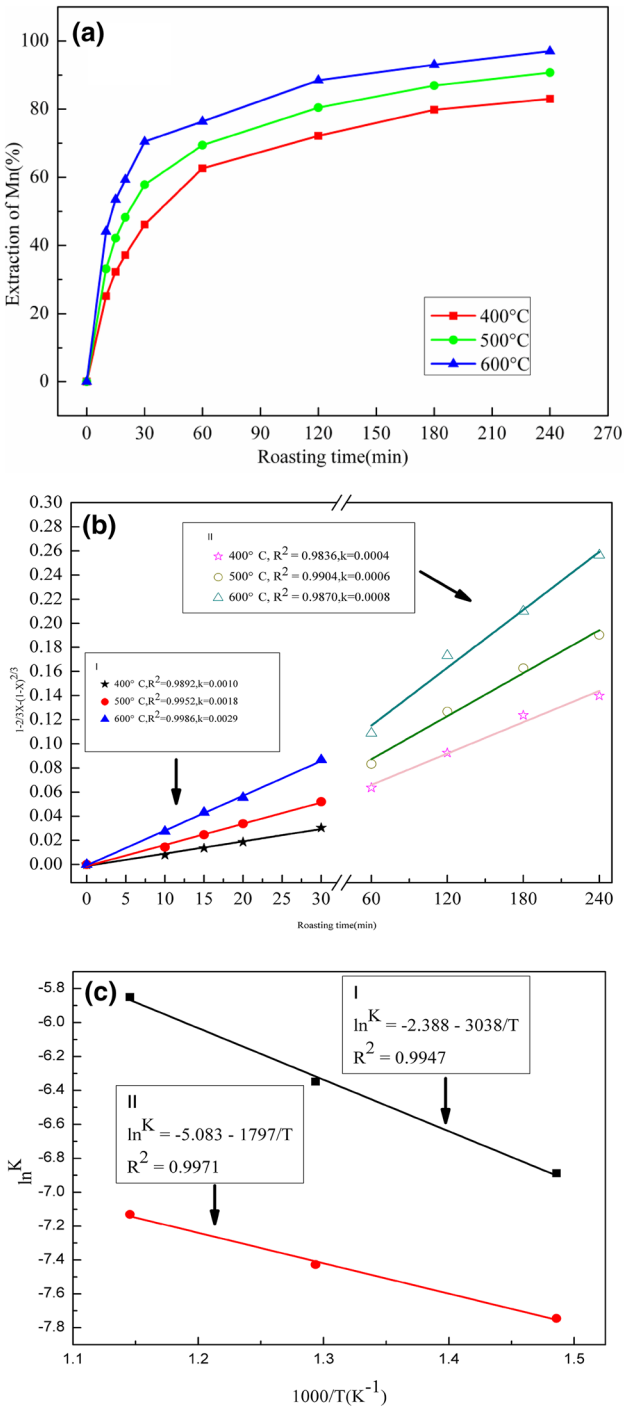

Fig. 4. (a) Relation between the extraction of Mn and time at different temperatures. (b) Relation between $1 - 2/3X - (1 - X)^{2/3}$ and time at different temperatures. (c) Relationship between ln$k$ and $1/T$.

Kinetic Analysis of the Roasting Process

The influence of the roasting temperature from 400°C to 600°C on the extraction of Mn was studied at a mass ratio of 2.0:1 of H_2SO_4 to pyrolusite and a volume ratio of 0.2:1 of H_2O to H_2SO_4 to obtain the roasting kinetic equations. The experimental results are shown in Fig. 4a. The extraction of Mn in the two periods from 0 min to 30 min and 60 min to 240 min was obviously different, so the kinetic data were divided into two parts for discussion. The roasting of pyrolusite with sulfuric acid can be modeled with a shrinking core model with a solid product layer. The simplified kinetic equations of the shrinking core model can be expressed as follows:[24]

$$x = k_f t \tag{7}$$

$$1 - 2/3x - (1 - x)^{2/3} = k_d t \tag{8}$$

$$1 - (1 - x)^{1/3} = k_r t \tag{9}$$

where X is the reaction ratio, K_f is the rate constant of external diffusion, K_d is the rate constant of internal diffusion, K_r is the rate constant of the chemical reaction-controlled process, and t is the reaction time.[25]

The experimental data in Fig. 4a were processed and fit to Eqs. (7), (8) and (9). As presented in Fig. 4b, Eq. (8) is the most suitable equation $1 - 2/3X - (1 - X)^{2/3}$ and the roasting time have a clear linear relationship in the two periods.

The relationship between the rate constant and temperature is given by the Arrhenius equation:

$$\ln k = \ln A - E/(RT) \tag{10}$$

where K is the rate constant, A is the frequency factor, E is the apparent activation energy, and R is the gas constant.[16]

The plots of ln$k$ versus $1/T$ are presented in Fig. 4c. The kinetic activation energy and pre-exponential factor can be determined from the slope and intercept of the line. The values are 25.26 kJ/mol and 9.18×10^{-2} min^{-1} in the time range of 0–30 min and 14.94 kJ/mol and 0.62×10^{-2} min^{-1} in the longer period from 60 min to 240 min. The kinetic equations can be expressed by Eqs. (11) and (12), respectively. The values of the apparent activation energy clearly verify that the roasting process of pyrolusite is controlled by internal diffusion. Compared to 60–240 min, the apparent activation energy of 0–30 min is greater. This is mainly because the reaction rate is proportional to the reactant concentration under internal diffusion control conditions. At the initiation of the reaction, the reactant concentration is higher and the reaction is faster; however, the reaction rate is slower because of the low concentration of reactants after 60 min.

$$1 - 2/3x - (1 - x)^{2/3} = 9.18 \times 10^{-2} \times \exp\left(-\frac{25260}{RT}\right)t \tag{11}$$

$$1 - 2/3x - (1-x)^{2/3} = 0.62 \times 10^{-2} \times \exp\left(-\frac{14940}{RT}\right)t \quad (12)$$

CONCLUSION

A roasting process for low-grade pyrolusite using H_2SO_4 followed by water leaching has been successfully demonstrated. The method was proven to be effective for developing and using low-grade pyrolusite. Both the H_2SO_4 addition and roasting temperature affect the extraction rate significantly. The experimental results indicated that a mass ratio of 2:1 of H_2SO_4 to pyrolusite, a roasting temperature of T = 650°C, a roasting time of 4 h and a volume ratio of 0.2:1 of H_2O to H_2SO_4 maximized the extraction rate of Mn at 98% and minimized the extraction rate of Fe at 1%. The technology can effectively extract manganese from low-grade pyrolusite. The kinetic analysis indicated that the roasting process follows a shrinking core model and is controlled by internal diffusion within the temperature range of 400–600°C. The apparent activation energies from 0 min to 30 min and from 60 min to 240 min were calculated to be 25.26 kJ/mol and 14.94 kJ/mol, respectively.

ACKNOWLEDGEMENTS

This work was funded by the National Natural Science Foundation of China (Nos. 51374056, 51404055, 51571054, 51674068), the Natural Science Foundation of Hebei Province (Nos. E2014501143, B20155010205), the Special Fund for Basic Scientific Research of Central Colleges, Northeastern University (Nos. N142304001, N142304002), Supporting Technology Project of Qinhuangdao Technology Bureau (No. 201501B015) and the Raining Foundation for Scientific Research of Talents Project, Hebei Province (No. A2016005004).

REFERENCES

1. B.P. Xin, T. Li, X. Li, Z.G. Dan, F.Y. Xu, N. Duan, Y.T. Zhang, and H.Y. Zhang, *J. Clean. Prod.* 92, 54 (2015).
2. Z.X. You, G.H. Li, Y.B. Zhang, Z.W. Peng, and T. Jiang, *Hydrometallurgy* 156, 225 (2015).
3. K.D. Yang, X.J. Ye, J. Su, H.F. Su, Y.F. Long, X.Y. Lv, and Y.X. Wen, *Trans. Nonferrous Met. Soc. China* 23, 548 (2013).
4. Z.L. Cai, Y.L. Feng, H.R. Li, X.W. Liu, and Z.C. Yang, *JOM* 64, 1296 (2012).
5. Z.L. Cai, Y.L. Feng, H.R. Li, Z.W. Du, and X.W. Liu, *Hydrometallurgy* 131–132, 40 (2013).
6. C. Acharya, R.N. Kar, and L.B. Sukla, *Miner. Eng.* 16, 1027 (2003).
7. Z. Cheng, G.C. Zhu, and Y.N. Zhao, *Hydrometallurgy* 96, 176 (2009).
8. Y.B. Zhang, Z.X. You, G.H. Li, and T. Jiang, *Hydrometallurgy* 133, 126 (2013).
9. M.S. Bafghi, A. Zakeri, Z. Ghasemi, and M. Adeli, *Hydrometallurgy* 90, 207 (2008).
10. X.F. Zhang, X.M. Tan, Y.J. Yi, W.Z. Liu, and C. Li, *JOM* 69, 2352 (2017).
11. F. Pagnanelli, G. Furlani, P. Valentini, F. Veglio, and L. Toro, *Hydrometallurgy* 75, 157 (2004).
12. H.F. Su, Y.X. Wen, F. Wang, Y.Y. Sun, and Z.F. Tong, *Hydrometallurgy* 93, 136 (2008).
13. D. Hariprasad, B. Dash, M.K. Ghosh, and S. Anand, *Miner. Eng.* 20, 1293 (2007).
14. R.N. Sahoo, P.K. Naik, and S.C. Das, *Hydrometallurgy* 62, 157 (2001).
15. Q. Tang, H. Zhong, S. Wang, J.Z. Li, and G.Y. Liu, *Trans. Nonferrous Met. Soc. China* 24, 861 (2014).
16. A.A. Nayl, I.M. Ismail, and H.F. Aly, *Int. J. Miner. Process.* 100, 116 (2011).
17. X.K. Tian, X.X. Wen, C. Yang, Y.J. Liang, Z.B. Pi, and Y.X. Wang, *Hydrometallurgy* 100, 157 (2010).
18. C.X. Li, H. Zhong, S. Wang, J.R. Xue, F.F. Wu, and Z.Y. Zhang, *Trans. Nonferrous Met. Soc. China* 25, 1677 (2015).
19. Z.G. Dan, Y.T. Zhang, J.H. Cai, X. Li, N. Duan, and B.P. Xin, *Int. J. Miner. Process.* 150, 24 (2016).
20. H.F. Su, Y.X. Wen, F. Wang, X.H. Li, and Z.F. Tong, *Miner. Eng.* 22, 207 (2009).
21. R.Z. Vracar and K.P. Cerovic, *Hydrometallurgy* 55, 80 (2000).
22. F.G. Buttler and A. Mitchell, *J. Therm. Anal.* 10, 257 (1976).
23. E.T. Turkdogan, R.G. Olsson, and J.V. Vinters, *Metall. Trans. B* 8, 60 (1977).
24. H.F. Su, H.K. Liu, F. Wang, X.Y. Lv, and Y.X. Wen, *Chin. J. Chem. Eng.* 18, 733 (2010).
25. J.R. Xue, H. Zhong, S. Wang, C.X. Li, J.Z. Li, and F.F. Wu, *J. Saudi Chem. Soc.* 20, 437 (2014).